

24 June 1995

RECEIVED

DEC 08 1995

OSTI

"Over the Horizon" SANS:

Measurements on Near-Surface Poiseuille Shear-Induced Ordering of Dilute Solutions of Threadlike Micelles

W.A. Hamilton^a, P.D. Butler^a, John B. Hayter^a, L.J. Magid^b and P.J. Kreke^b

^aNeutron Scattering Group, Oak Ridge National Laboratory, Oak Ridge, TN 37831-6393, USA.

^bDepartment of Chemistry, University of Tennessee, Knoxville, TN 37996-1600, USA.

Although the behavior of a fluid under shear near a surface can be expected to be critically important to its drag and lubrication properties, most shear measurements to date have been of the bulk. This paper outlines the use of a specially developed Poiseuille shear cell at grazing incidence to measure the small-angle neutron scattering (SANS) signal from the first few tens of microns in the interfacial region. We illustrate the technique with measurements made on the near-surface ordering in flow past a quartz surface of dilute surfactant solutions comprising highly extended self-assembling "threadlike" micelles.

Keywords: micelles, Poiseuille shear, SANS

Corresponding author:

W. A. Hamilton

Phone: 1 (615) 576-6068

Bldg 7962, Mail stop 6393

FAX: 1 (615) 574-6268

Neutron Scattering Group

Email: HW5@ORNL.GOV

Oak Ridge National Laboratory

Oak Ridge, TN 37831-6393, USA

MASTER

"The submitted manuscript has been authored by a contractor of the U.S. Government under contract No. DE-AC05-84OR21400. Accordingly, the U.S. Government retains a nonexclusive, royalty-free license to publish or reproduce the published form of this contribution, or allow others to do so, for U.S. Government purposes."

DISTRIBUTION OF THIS DOCUMENT IS UNLIMITED

DISCLAIMER

Portions of this document may be illegible in electronic image products. Images are produced from the best available original document.

1. Introduction

In flow past a surface a strong geometrical constraint is added to the anisotropy imposed by shear. In some "near-surface" region the effects of this constraint and interactions with the surface will strongly affect the structural morphology within the solution, modifying or even changing the phase from that induced in a bulk shear field. To date most structural measurements of fluids under shear flow have been, for technical reasons, of bulk behavior. However, many important properties of flowing systems, for instance drag and lubrication, clearly depend critically on behavior near an interface. A specially developed Poiseuille geometry cell allows the investigation of the near-surface properties of solutions under flow past a quartz slab surface by measuring the neutrons small-angle scattered back toward the solid-liquid interface of a neutron beam refracted into the solution at grazing incidence. For usual liquid transmissions this scattering back over the interfacial "horizon" allows us to probe the high shear region near the interface to a depth of a few tens of micron. Data taken using this cell has previously provided clear evidence of Poiseuille shear-induced near-surface hexagonal ordering in a dilute solution of charged threadlike micelles under flow. Using these measurements we outline the necessary corrections to SANS data taken in this highly refractive geometry and illustrate some of the possibilities of the technique.

2. Couette and Poiseuille shear

The major advantages and characteristics of a reflection geometry cell for the scattering investigations of shear-induced phases in flowing systems are evident from a study of figure 1, which compares the scattering geometry with that of the widely used Couette shear cell, in which the fluid is sheared in the annular region between a (usually) stationary inner cylinder and an outer cylinder which rotates [1]. Although the cylindrically

symmetric Couette cell is well suited for the case (A) of scattering measurements with Q roughly perpendicular to the shear gradient direction, ∇ , obvious problems occur even in bulk measurements for the case (B) when the scattering vector is near perpendicular to the flow direction, V , requiring that the incident neutron beam be nearly parallel to V . For a neutron beam collimated to the width of the Couette gap, t , the flow direction in the volume of sample probed varies through an angle $\sim 2\sqrt{(2t/r)}$, where r is the radius of the sample annulus. For typical values of t and r , say 0.5-1.0 mm and 25 mm, this variation will be of order 10-20°, smearing out any measurement of the anisotropy of the sample. To study the near-surface shear region in this case a narrow beam must be aimed at a region of the solution close to the surface of the outer rotating cylinder. The costs in beam intensity and effective sample volume in this situation are severe. Moreover, since the beam passes at near grazing incidence to the curved solution-cylinder interface low angle refraction effects vary rapidly across even a narrow beam and are difficult to estimate and correct for properly. Strong mirror reflection of the beam will also occur over a range of angles near the critical angle for the interface giving rise to a fan of specularly reflected neutrons masking the scattering signal.

In the Poiseuille case, the fluid is sheared as it moves past the planar surface of a solid slab from within which the neutron beam is incident at grazing angles. The geometry of the problem is Cartesian and the shear gradient, flow direction and sample surface have a constant orientation to the incident neutron beam approximating case (B) above (case (A) would have the beam nearly perpendicular to the plane of the page). We probe the near-surface region by measuring the small-angle neutron scattering signal from the beam refracted into fluid above the critical angle for total neutron reflection. For typical macroscopic neutron cross-sections ($\sim 1\text{cm}^{-1}$) and grazing angles ($\lesssim 1^\circ$) the incident beam penetrates to depths of only a few tens of microns in the near-surface region. Although this region is deeper than we might probe with specular neutron reflectometry ($\sim 0.5\mu\text{m}$) or

evanescent wave scattering ($\sim 100\text{\AA}$), it is still within the depth we might expect to be strongly affected by the presence of the interface for colloidal systems containing highly extended structures and much thinner than that accessible with neutron scattering in a Couette cell. The sample volume can easily be increased by increasing the length of the interface and, since the orientation is constant within the sample volume, refraction, transmission and reflection corrections due to passage through the solid-liquid interface depend relatively simply on the scattering angle. Specular reflection from the interface, although still a strong signal which can overwhelm the scattered signal from within the solution, can be steered from regions of interest by changing the angle of incidence to the interface. It can even be a useful normalization; since the total cross-section represented by the specular signal is equal to the (easily measured [2,3]) specular reflectivity by the exposed area of the interface.

3. Poiseuille shear cell

A schematic diagram of the shear cell (which is described in detail elsewhere [4]) used in these experiments is shown in figure 2(a). The solution under study is pumped in closed cycle through a 1 mm deep, 5.5 cm wide channel 10 cm long formed in a block of teflon beneath a polished slab of crystalline quartz. To facilitate the rapid development of even laminar flow across the cell, the fluid enters the channel through a row of evenly spaced small holes below which is a large diameter reservoir to damp turbulence and equalize the inlet pressure. At the far end of the channel fluid exits through a full width slit in a similar reservoir. To block scattering from the teflon block its leading and trailing faces are covered with cadmium. Neutrons scattered to the detector are either the product of specular reflection at the solid-liquid interface, or have undergone: refraction upon transmission through this interface, a scattering event deflecting them back toward the interface, and a final refraction upon transmission into the quartz. This is shown schematically in figure 2(b), in which the notation for the various beam wavevectors and

scattering vectors is also defined. The angles of the beams to the interface have been greatly exaggerated, in the present measurements they are less than a few degrees. The scattered beams are also within a few degrees of the reflection plane, defined by the incident and specularly reflected beams. Neutrons therefore enter and exit the cell nearly perpendicular to the leading and trailing faces of the quartz slab, consequently there is no significant reflection or refraction at these boundaries.

Figure 2(c) shows a schematic of the scattering and SANS detector geometry for our Poiseuille cell measurements. In addition to a goniometer mounting allowing variation of the neutron beam's (grazing) angle of incidence to the interface, θ_i , the cell is directly mounted on stage giving rotation about an axis normal to the interface, ω , allowing independent variation of the incident beam's angle to the flow direction.

4. Threadlike micellar systems

Some of the most interesting complex fluid characteristics are exhibited by aqueous solutions of certain ionic surfactants, molecules in which a non-polar hydrocarbon "tail" is chemically bonded to a charged "head", aggregate into cylindrical micellar structures. In these supramolecular structures a layer of the charged head groups surrounds a core of the non-polar tails. In some cases these micelles are so highly extended, "threadlike" in that their lengths are many hundreds or even thousands of times their diameters, that even dilute solutions, with volume fractions less than 0.1%, are above the overlap concentration (c^*) at which interaction between micelles will become significant.

To a first approximation semi-flexible cylindrical micelles in solution may be treated theoretically as high molecular weight polymers [5]. However, critical differences obviously exist. The micelles being self-assembling structures are

transient rather than permanent, constantly breaking and recombining [6]. The micellar diameter is relatively large (at roughly twice the extended length of the hydrocarbon tail) in comparison to typical polymer backbones making them considerably stiffer than typical flexible polymers. Also, in systems such as those discussed here incomplete binding of the associated counterions to the micellar surface can give these structures a significant surface charge density, resulting in electrostatic forces between micelles of much longer range than the "contact" interactions in an uncharged entangled system. These systems members are then members of the class of linear polyelectrolytes - a group which also includes nucleic acids as well as many other systems of biological and technological interest. Elucidation of the microstructure and complex fluid dynamics exhibited by such systems at rest and under shear is a challenging area of considerable theoretical, experimental and practical interest.

Our Poiseuille shear cell measurements have focused on systems containing the cationic surfactant cetyltrimethylammonium 3,5-dichlorobenzoate (CTA3,5ClBz). In aqueous solution this surfactant forms very long threadlike micelles having a diameter of 46 nm. Cryo-TEM images [7] of vitrified aqueous micellar solutions of this surfactant show a network of micelles, with contour lengths on the order of many 100's of nm, which is already highly entangled at volume fractions of 0.1% (~2mM), a factor of ten lower than the concentrations studied in the present work. These liquids are strongly viscoelastic; since, like an elastic solid, the interacting micellar mesh is able to support finite shear. A 20 mM solution, at over 20 times c^* , is a Maxwell fluid with a relaxation time ~500 s and a zero shear viscosity of 1200 Pa.s, about 10^6 times that of water. However, under flow the solution shears dramatically. The relationship of the shear stress to the shear strain follows a power law dependence, $\dot{\gamma} = dv/dz$, with a coefficient α of 0.05 ($\alpha=1$ for Newtonian

fluids) [8]. The solution's viscosity therefore falls as $\sim 1/\dot{\gamma}^{0.95}$. For power law behavior of viscosity at small α shear rates are large over a thin boundary layer near channel walls and most of the fluid will travel through a constant width channel as a "plug" at a speed close to the average $\langle v \rangle$. The flow velocity in a channel will rise from zero at the walls (assuming no slip) to one half its maximum over a depth $\sim \alpha t/4\ln 2$, where t is the full depth of the channel [9]. For $\alpha=0.05$ and $t=1$ mm this distance will be about 20 μm , and we may estimate the average shear $\langle \dot{\gamma} \rangle$ rate over this depth in our cell to be about 20 times the numerical velocity of $\langle v \rangle$ in mms^{-1} . A full analysis of the dynamic rheological measurements [10] provides further information about the micellar network indicating that the micelles have a persistence length (i.e. minimum radius of curvature) of 40-60 nm, and a contour length between mesh entanglement points of 250 nm.

The binding of the $3,5\text{ClBz}^-$ counterions to the micellar surface is about 90%, so the charges of the (trimethylammonium, $\text{N}(\text{CH}_3)_3^+$) head groups are not fully neutralized, resulting an excess charge along a micelle of about $+2e \text{ nm}^{-1}$. We have further found that the micellar charge density can be tuned (increased) by replacing a portion of the 3,5-dichlorobenzoate counterions with bromide ions, which increases the extent of counterion dissociation. The two systems discussed here are the homogeneous counterion (HC) system with 20mM of $\text{CTA}_{3,5\text{ClBz}}$, and a mixed counterion (MC) system containing 14mM $\text{CTA}_{3,5\text{ClBz}}$ and 6mM CTABr , making it 70 mol% in $\text{CTA}_{3,5\text{ClBz}}$ (70/30 MC). In addition to increasing the strength of the electrostatic interaction between micelles, increasing the surface charge density will also increase the self-repulsion of a micelle along its length. The micelle will therefore be less flexible resulting in a longer persistence length, allowing the micelle to curve less between entanglement points.

Our bulk scattering measurements [11] have shown that under Couette shear the micelles of these systems align with their long axes along the flow direction, as do many of similar morphology [12,13]. We have also found that, as we might expect, the less flexible, more strongly interacting MC systems align more readily under shear than the HC systems. As is evident from the Couette shear data presented in figure 3, full alignment of the 70/30 MC system was observed at shear rates of $\dot{\gamma}=10 \text{ s}^{-1}$, while the HC system is only partially aligned at 20 s^{-1} . Saturation of the anisotropic signal for the HC system required rates about an order of magnitude higher.

5. Poiseuille cell scattering data 70/30 MC system

The Poiseuille cell small-angle scattering measurements made so far have used the 30 m SANS Facility at the Oak Ridge National Laboratory [14] using neutrons of wavelength $\lambda=4.75 \text{ \AA}$. The solvent for our samples is actually D_2O to maximize the neutron contrast with the micelles. The average coherent scattering length density for these dilute solutions, β_S , is within a few percent of that of pure D_2O , $6.4 \times 10^{-6} \text{ \AA}^{-2}$. The scattering length density for the quartz, β_Q , is $4.2 \times 10^{-6} \text{ \AA}^{-2}$. The critical angle for total external reflection at the interface is 0.23° , $\sin^2 \theta_C \equiv \lambda^2 (\beta_S - \beta_Q) / \pi$, corresponding to a critical specular wave vector transfer of 0.010 \AA^{-1} , $Q_C^2 \equiv 16\pi(\beta_S - \beta_Q)$. For the measurement presented here the neutron beam was incident at $\theta_i=0.3^\circ$, corresponding to a specular wave vector transfer Q_R of 0.014 \AA^{-1} , for which values the reflection coefficient at the quartz-solution interface has fallen to $\sim 8\%$; so most of the neutrons incident at the interface will be refracted into the solution to probe the interfacial region.

Figure 4(a) shows a 1.5 hr raw data set for the 20 mM 70/30 MC system under static conditions. Although some weak scattering is apparent over the interfacial

horizon, the overwhelming dominant signal is the specularly reflected beam at Q_R . Figure 4(b) shows the scattering pattern observed over 9 hr for a mean flow velocity through the channel of $\langle v \rangle = 8 \text{ mms}^{-1}$, corresponding to a rate of shear near the interface $\langle \dot{\gamma} \rangle \sim 150 \text{ s}^{-1}$. The specular reflection signal is now surrounded by a Bragg diffraction pattern clearly indicating scattering of the beam transmitted into the solution by a shear induced "crystalline" phase in the interfacial region. In addition to aligning along the flow direction the micelles near the surface are ordered in a regular triangular array strongly oriented with respect to the quartz surface.

6. Cross-section corrections

The necessary corrections necessary to obtain the macroscopic differential scattering cross-section $d\Sigma/d\Omega'$ of the in-solution scattering from measurements such as these are rather different to those employed in conventional SANS. Owing to our grazing incidence scattering geometry transmission measurements cannot be made for the sample in our cell, precluding absolute cross-section normalization against known standards [15]. To obtain the scattering vector in-solution Q' from the observed scattering vector Q , we must correct for the refraction of the neutron beam upon entering and leaving the solution through the interface. Refraction will also distort the solid angle into which the beam was scattered in solution. Further, correction must be made for absorption averaged over possible paths in both quartz slab and the solution as well as for transmissions on passing across the interface.

In answer to the first of these problems, we note that the presence of the specularly reflected beam in this data set presents the opportunity of a relatively simple absolute normalization of the cross-section data. The quartz-solution interface presents an cross-section acceptance of: $A = W L_s \sin \theta_i$, where L_s is the length of the flow channel and W the beam width at the sample (set by a 0.8 cm

guard aperture in our measurements); 0.042 cm^2 at an incident angle of 0.3° . Using the measured specular reflectivity for the interface 8% at $Q_R = 0.014 \text{ \AA}^{-1}$ (graph figure 5), and allowing for the measured transmission through the quartz for 4.75 \AA of 70%, we can calculate that the integrated specular signal in the data set represents a total cross-section of 0.005 cm^2 . Normalizing the data set to this value agreed to within 20% with that obtained from a neutron flux measurement at the SANS sample position [16].

Since only the components of the neutron wavevector perpendicular to the surface are affected on refraction we see that only the component of \mathbf{Q}' normal to the interface is changed. The incident and final wavevectors components in the solution (primed) and in the quartz are related as:

$$\begin{aligned} \mathbf{k}'_i \cdot \hat{\mathbf{n}} &= -\sqrt{(\mathbf{k}_i \cdot \hat{\mathbf{n}})^2 - 4\pi(\beta_S - \beta_Q)} \\ \mathbf{k}'_f \cdot \hat{\mathbf{n}} &= \sqrt{(\mathbf{k}_f \cdot \hat{\mathbf{n}})^2 - 4\pi(\beta_S - \beta_Q)} = \sqrt{((\mathbf{k}_i + \mathbf{Q}) \cdot \hat{\mathbf{n}})^2 - 4\pi(\beta_S - \beta_Q)} \end{aligned} \quad (1)$$

where $\hat{\mathbf{n}}$ is the interface normal. The corresponding angles to the interface for the various beams will be related as:

$$\begin{aligned} \sin^2 \theta'_i &= \sqrt{\sin^2 \theta_i - \sin^2 \theta_C} \\ \sin^2 \theta'_f &= \sqrt{\sin^2 \theta_f - \sin^2 \theta_C} \end{aligned} \quad (2)$$

It is convenient for data reduction purposes to cast these refraction corrections in terms of Q_C and scattering vector for a data set's specularly reflected signal, Q_R , for which: $\mathbf{Q}_R = -2\mathbf{k}_i \cdot \hat{\mathbf{n}}$ and $\hat{Q}_R = \hat{\mathbf{n}}$. We may then write the refraction transform from the observed scattering vector to the (primed) in-solution scattering vector as:

$$Q' = Q + \hat{Q}_R \left[-Q \cdot \hat{Q}_R + \sqrt{(Q \cdot \hat{Q}_R - Q_R/2)^2 - (Q_C/2)^2} + \sqrt{(Q_R/2)^2 - (Q_C/2)^2} \right] \quad (3)$$

The ranges of scattering observed from the solution are defined by the real roots in this expression. From the first square root term we find that the apparent horizon for the minimum observed in-solution scattering normal to the interface is:

$$Q \cdot \hat{Q}_R \geq (Q_R + Q_C)/2 \quad (4)$$

That is, the k_f beam makes an angle at least θ_C to the quartz-solution interface, so the minimum observed scattering deflection normal to the interface will be $\theta_i + \theta_C$. This horizon for scattering from within the fluid is clearly visible in figure 4(b). The second term indicates that to see in-solution scattering the neutron beam must be incident upon the interface at angle above that for total reflection, i.e. the obvious, that there must be a beam transmitted into the solution. Also it is the lower limit on the experimentally accessible in-solution scattering normal to the interface. So we have:

$$Q \cdot \hat{Q}_R \geq \sqrt{(Q_R/2)^2 - (Q_C/2)^2} \quad (5)$$

In terms of the beam direction within the solution, this simply requires that the in-solution scattering must send the beam back toward the interface.

As noted previously, the refraction of the neutron beam as it exits the solution will change the element of solid angle into which it is scattered. For small-angle

scattering in our geometry the ratio of elements of solid angle at the detector and in the solution is given to a good approximation by:

$$\frac{d\Omega}{d\Omega'} \equiv \frac{d(\mathbf{Q} \cdot \hat{\mathbf{Q}}_R)}{d(\mathbf{Q}' \cdot \hat{\mathbf{Q}}_R)} = \frac{\sqrt{(\mathbf{Q} \cdot \hat{\mathbf{Q}}_R - Q_R/2)^2 - (Q_C/2)^2}}{\mathbf{Q} \cdot \hat{\mathbf{Q}}_R - Q_R/2} \quad (6)$$

In terms of beam angles to the interface this factor is $\sin\theta'_f/\sin\theta_f$. When the normal component of the transfer normal to the interface is close to its minimum, θ_f is just above θ_C , this value will be rather less than unity. Due to refraction a detector cell in this region will subtend a much larger solid angle $\Delta\Omega'$ as "seen" from within the solution than we would normally calculate and the degradation of resolution will be pronounced. The calculated variation of this factor for the data set is shown in the graph figure 5.

It is also necessary to correct for the reduction of incident beam in the solution due to reflection at the interface as the neutron beam enters the flow channel from the quartz and for reflection as neutrons scattered within the solution exit. This correction factor is simply calculated from a measurement of the specular reflection coefficient. The transmission coefficient for beam current into the solution is simply $T(Q_R)=1-R(Q_R)$. The transmission factor for the scattered beam leaving the solution is obtained using Stokes relations for reflection and refraction: in the absence of significant absorption at the interface, transmission across the interface is unchanged by reversal of the direction of propagation. So the exit transmission factor may be obtained from the specular reflectivity we would measure for a beam incident upon the quartz-solution interface at θ_f . In terms of the measured Q values for a data set

the total interfacial transmission correction factor can therefore be obtained from the measured specular reflectivity R at the interface:

$$\left[T(Q_R)T(\mathbf{Q} \cdot \hat{Q}_R - Q_R/2) \right]^{-1} \cong \left[(1 - R(Q_R))(1 - R(\mathbf{Q} \cdot \hat{Q}_R - Q_R/2)) \right]^{-1} \quad (7)$$

The variation of this factor calculated from the measured specular reflectivity for the 20 mM 70/30 MC in the graph figure 5. As is evident from the figure the variation of this factor roughly cancels that of the solid angle correction (for sharp edge Fresnel reflection the cancellation would be nearly exact in the region of rapid variation just above the scattering horizon).

In contrast to a conventional SANS measurement, the total volume of sample which contributes to the scattered signal at a given Q' is dependent on the scattering angle. Since the scattered beams are within a few degrees of the specular reflection plane, we see from figure 6 that the geometrically possible volume may be given to a good approximation by:

$$V(\theta_f) \cong \frac{1}{2} W L_S^2 / [1/\tan \theta_i + 1/\tan \theta_f] \quad (8)$$

This is simply the volume of a solid prism of the beam width by the area of the triangle between the interface and the maximum path in the solution at this angle, for a neutron entering the solution immediately past the fluid seal behind the leading cadmium stop and exiting immediately before the seal at the trailing stop. Of course, there will be a negligible signal contribution from a path anywhere near this of this length through the solution. Since the triangle is shallow such a neutron would travel almost exactly the 100 mm length of the flow cell in the solution, over 8

times the measured $1/e$ absorption length for our solutions 1.2 cm. Only neutrons following paths of the same angle, but entering and leaving the solution after traveling less than a few cm and traversing the rest of the distance through the cell in the quartz ($1/e$ length = 33 cm) will contribute significantly to the signal at this scattering vector. Consequently, the measured scattering cross-section at each Q' must be normalized to the a scattering volume averaged for transmission. As is shown in figure 6 the contributing element of sample volume at a depth z in the solution will have a volume:

$$dV(\theta'_f) \cong dzW(L_S - z/[1/\tan \theta'_i + 1/\tan \theta'_f]) \quad (9)$$

Since the path is shallow the distance traveled in the solution by a neutron scattered at this depth will be very close to the length of the triangle, that is $z/[1/\tan \theta'_i + 1/\tan \theta'_f]$, while for the rest of its full path through the cell L_Q (12 cm) the neutron beam travels through the quartz slab. The bulk absorption coefficients of the solutions and the crystalline quartz for 4.75 Å neutrons, μ_S and μ_Q , were determined from conventional SANS transmission measurements to be 0.86 cm^{-1} and 0.030 cm^{-1} respectively. Integrating over the element of sample volume by the absorption for a neutron path scattering at that depth, we may show that the effective volume corrected for absorption in the solution and the quartz is given by:

$$V'_{\theta'_f} \cong V_{\theta'_f} e^{-\mu_Q(L_Q - L_S)} 2 \left[e^{-\mu_S L_S} + ([\mu_S - \mu_Q] L_S - 1) e^{-\mu_Q L_S} \right] / ([\mu_S - \mu_Q] L_S)^2 \quad (10)$$

The first exponential term in this equation simply represents the transmission over the (20 mm) distance a neutron must travel in the quartz since it overlaps the flow channel (94%). The remaining factor represents the effective fraction of the possible

solution volume which contributes to our scattering signal, $\sim 15\%$ at any scattering angle, so the depth probed in our measurements is only about 8% of the depth of the maximum path. For the data shown in figure 4 this effective volume will vary from about 0.02 cm^3 , depth probed $\approx 30 \text{ }\mu\text{m}$, high on the detector to about 0.01 cm^3 , $\approx 15 \text{ }\mu\text{m}$, at the level of reflected beam.

5. Shear-induced near-surface ordering

After correcting for the effects outlined in the preceding section the change in differential macroscopic cross-section $\Delta(d\Sigma/d\Omega')$ between flow on and flow off 20 mM 70/MC data sets is shown in figure 7. After refraction correction this difference signal clearly shows several orders of diffraction from what is, within experimental error, an undistorted hexagonal pattern. From it we may directly infer that the micelles near the surface are not only aligned along the flow direction as the Couette data indicate, but also ordered in a hexagonal array with a nearest neighbor separation of 370 \AA (inset figure 7). Since the micelles are charged this will represent a minimum of their electrostatic potential energy. This reduced data set has been discussed in detail previously [17], here we note the implications of this shear-induced crystalline structure to the surface for of the shear thinning characteristics of this solution. If we can assume that the shear gradient induces this ordering is smoothly varying, planes of micelles separated by 320 \AA in depth are passing each other at many thousand \AA s^{-1} . The regular well oriented micellar arrangement indicated by this data (the tangential width of the diffraction spots is $\sim 30^\circ$ FWHM) minimizes their interference with the surface and each other under shear.

The diffraction spots we observe have a mosaic width determined by convolution of finite micelle length effects with the distribution of "crystallite" orientations in the sample. The severity of the refraction corrections make it very difficult to perform rocking curve measurements involving a change in the angle of incidence of beams to the surface. This

and reflected beam interference precludes measurement on the strong **01** spot. However, rotation about the surface normal (ω axis) does not change angles of any scattered beams to the surface, so measurements were possible for the other visible first order spots, the **10** and **11**, despite their proximity to the scattering horizon (figure 8). After correction for the 30° angle between the rotation axis and the normal to the scattering plane we obtain a very respectable $4\text{-}5^\circ$ mosaic. Assuming this is a size effect sets a lower limit of $\sim 3000 \text{ \AA}$ on the micellar length. However, neutron and light scattering observations of static solutions as well as rheological measurements all indicate the micelles are much longer than this, so the width is presumably largely due to rippling of the micellar structure as the fluid moves past the quartz surface.

As expected from the Couette SANS data the HC system proves rather more difficult to align under Poiseuille shear than the MC system. Figure 9 shows corrected $\Delta(d\Sigma/d\Omega')$ data for the 20 mM HC system at a flow rate $\langle v \rangle = 20 \text{ mms}^{-1}$, corresponding to a rate of shear $\langle \dot{\gamma} \rangle \sim 400 \text{ s}^{-1}$. Away from the reflected beam region this data shows only a very weak arc of scattering, over an order of magnitude less intense than the first order diffraction signal for the MC data. Interpretation of so weak a signal is difficult, but the data seem consistent with a 2D liquid or possibly layered structure. Similar effects have been observed for the MC system when the electrostatic interaction between micelles is weakened upon the addition of supporting electrolyte, decreasing the Debye screening length in the solution. Experiments are currently underway to track the disruption of the MC system's crystalline ordering by this means through a series of rocking curve measurements.

6. Conclusion

The power of our SANS technique using the Poiseuille geometry cell is best exemplified in the rocking curve data presented in figure 8, in that we have been able to obtain and

interpret scattering measurements which amount to performing "single" crystal diffraction on a flowing system. A large number of possibilities arise naturally from the data and the correction analysis presented here. Perhaps the most obvious for the systems discussed is control of the depth probed by the technique by using mixtures of H₂O ($\mu=6.2 \text{ cm}^{-1}$ at 4.75 \AA) and D₂O ($\mu=0.8 \text{ cm}^{-1}$ at 4.75 \AA) as the solvent; at the expense of some (calculable) loss of contrast. The analysis presented here assumes that the ordering of the micellar system is saturated over $10\text{-}30 \text{ }\mu\text{m}$. The relative weakness of the near-surface signal for the HC system may well be due to the fact that an ordered structure does not extend over this depth. At a given flow rate, measurements at a series of H₂O solvent fractions might provide an answer to this question. The refraction corrections to in-solution scattering in the systems discussed would obviously be reduced in severity if the overlying slab were index matched to the solution. A smaller cell design using a sapphire slab, which has a scattering length density close to that of D₂O has been built and short preliminary measurements made for the HC system, which also benefits from lower interference from the weakened specular reflection signal. For both these systems full specular reflection profile measurements taken on the reflectometers MIRROR at ORNL and SPEAR at the Los Alamos National Laboratory [18], suggest the presence of a layer of adsorbed surfactant layer $20\text{-}30 \text{ \AA}$ thick at the quartz surface. Due to the incomplete counterion binding such a layer should create an effective charge sheet at the quartz-solution interface. Integration of the specular and SANS data should allow the investigation of the structural consequences we would expect due to the interaction between this adsorbed layer and the shear-induced phases in the flow. Finally, we note that near-surface effects akin to those presented here should also be present in other complex fluid systems of similar morphology, for example solutions of high molecular weight polymers.

Acknowledgments

This work was supported by the U.S. DOE Division of Materials Sciences under contract DE-AC05-84OR21400 with Martin Marietta Energy Systems. The Poiseuille shear cell was designed in collaboration with S.M. Baker, G.S. Smith, R. Pynn and R. Sanchez of Los Alamos National Laboratory. The HC system SANS data presented in figure 2 were taken at National Institute of Standards and Technology in collaboration with B. Hammouda using the NG3 instrument which is supported by the NSF under agreement DMR9122444.

-
- [1] For example: P. Lindner and R. Oberthür, *Rev. Phys. Appl.* 19 (1984) 663.
 - [2] Reviews: J. Penfold and R.K. Thomas, *J. Phys.: Condens Matter* 2 (1990) 1369; and T.P. Russell, *Materials Science Reports* 5 (1990) 171.
 - [3] W. A. Hamilton, J. B. Hayter, and G. S. Smith, *J. Neutron Research.* 2 (1994) 1.
 - [4] S.M. Baker, G.S. Smith, P.D. Butler, J.B. Hayter, W.A. Hamilton, L.J. Magid and R. Pynn, *Rev. Sci. Inst.* 65 (1994) 412.
 - [5] P.G. de Gennes, *Scaling Concepts in Polymer Physics* (Cornell University Press, Ithaca, NY, 1979) Chap. VIII.
 - [6] See for instance: M.E. Cates and S.J. Candau, *J.Phys.: Condens. Matter* 2 (1990) 6869; and references therein.
 - [7] L. J. Magid, J. C. Gee, and Y. Talmon, *Langmuir* 6 (1990) 1609.
 - [8] Unpublished Couette viscometer measurements by T.L. Smith and L.J. Magid.
 - [9] R.J. Hunter, *Foundations of Colloid Science* (Clarendon, Oxford, 1989), Vol. II, Chap. 18.
 - [10] See: R. Granek and M.E. Cates, *J. Chem. Phys.* 96 (1992); and [6].
 - [11] P.D. Butler, L.J. Magid, P.J. Kreke, J.B. Hayter and B. Hammouda, "Novel Kinetic Effects in Viscoelastic Surfactant solutions Under Shear", *Materials Research Society Symposium Proceedings* (in press).

-
- [12] J.B. Hayter and J. Penfold, *J. Phys. Chem.* 88 (1984) 4589.
- [13] V.K. Jindal, J. Kalus, H. Pils, H. Hoffman and P. Lindner, *J. Phys. Chem.* 94 (1990) 3129; Ch. Münch, H. Hoffman, K. Ibel, J. Kalus, G. Neubauer, U. Schmelzer and J. Selbach, *J. Phys. Chem.* 97 (1993) 4514.
- [14] W.C. Koehler, *Physica B* 137 (1986) 320.
- [15] W.S. Dubner, J.M. Schulz and G.D. Wignall, *J. Appl. Cryst.* 23 (1990) 469.
- [16] This discrepancy was probably due, for the most part, to the difficulty of estimating the relative sensitivities of the single ^3He tube detector used for the sample position flux measurement and the 2D multiwire SANS detector. On balance, the specular reflection signal cross-section method which normalizes to unit reflectivity below the critical edge would seem simpler and more reliable in this scattering geometry.
- [17] W.A. Hamilton, P.D. Butler, S.M. Baker, G.S. Smith, J.B. Hayter, L.J. Magid and R. Pynn, *Phys. Rev. Lett.* 72 (1994) 2219; Erratum: *Phys. Rev. Lett.* 74 (1995) 335.
- [18] In collaboration with G.S. Smith, S.M. Baker and R.Pynn.

DISCLAIMER

This report was prepared as an account of work sponsored by an agency of the United States Government. Neither the United States Government nor any agency thereof, nor any of their employees, makes any warranty, express or implied, or assumes any legal liability or responsibility for the accuracy, completeness, or usefulness of any information, apparatus, product, or process disclosed, or represents that its use would not infringe privately owned rights. Reference herein to any specific commercial product, process, or service by trade name, trademark, manufacturer, or otherwise does not necessarily constitute or imply its endorsement, recommendation, or favoring by the United States Government or any agency thereof. The views and opinions of authors expressed herein do not necessarily state or reflect those of the United States Government or any agency thereof.

FIGURE CAPTIONS

Fig 1. Scattering geometries for Couette and Poiseuille shear cells.

Fig. 2. (a) Schematic of Poiseuille cell. (b) Scattering geometry for insolution scattering. Angles of beam wavevectors to the interface are greatly exaggerated. Note that while the scattered beams, k_f and k'_f , are always within a few degrees of the specular reflection plane (containing k_i , k'_i , k_R , and Q_R) this is not true of the scattering vectors Q and Q' . (c) Schematic of the scattering and SANS detector geometry for Poiseuille cell measurements.

Fig. 3. Couette bulk shear cell SANS data for the 20 mM 70/30 MC and HC systems. The patterns are 0.08 \AA^{-1} on a side. The scattering geometry is as shown for figure 1 case A. As the micelles align structure factor correlations peak perpendicular to the the flow direction. (The MC measurements were made at ORNL on the 30 m SANS, while the HC measurements were made using the SANS instrument NG3 at NIST.)

Fig. 4. Poiseuille cell scattering patterns for the 20 mM 70/30 MC system. (a) Static and (b) at a channel flow velocity $\langle v \rangle = 8 \text{ mms}^{-1}$, corresponding to a shear rate $\dot{\gamma} \sim 80 \text{ s}^{-1}$. The patterns are 0.1 \AA^{-1} on a side. The \times marks $Q=0$.

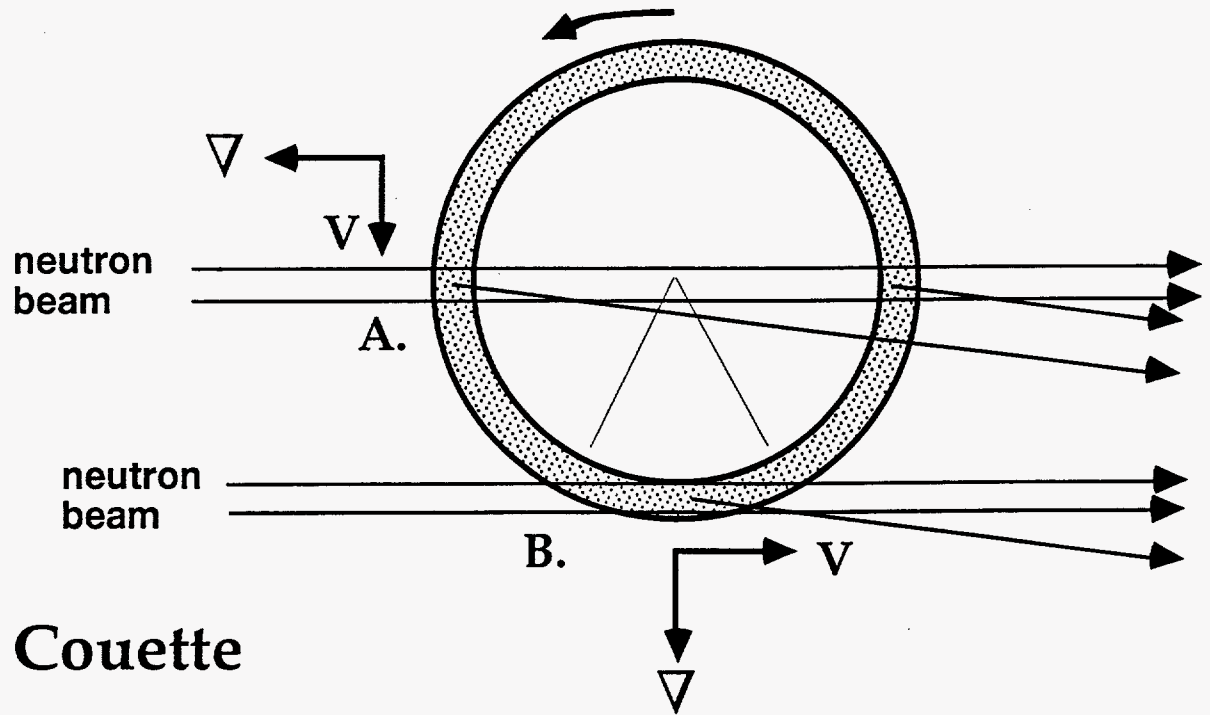
Fig. 5. Variation of cross-section correction factors discussed in the text. The interfacial transmission correction factor for the data in figure 4 is calculated from the specular reflectivity shown. The specular measurements were made on the MIRROR neutron reflectometer at ORNL.

Fig. 6. Cell schematic showing volume element contributing to signal at a given scattering vector at a depth z from the interface.

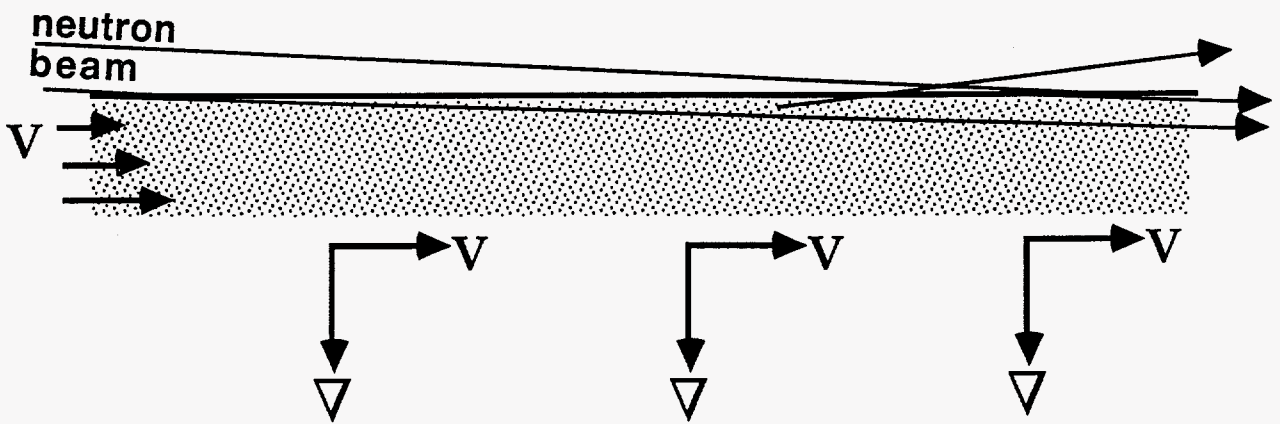
Fig. 7. Flow on minus flow off $\Delta(d\Sigma/d\Omega')$ differential cross-section for insolution scattering for 20 mM 70/30 MC system shown in figure 4. (Contours are factors of $\sqrt{2}$ on once smoothed data.) Inset shows hexagonal indexing of the observed diffraction spots. Cartoon shows a schematic of the hexagonal micellar alignment near the interface under flow.

Fig. 8 Rocking curve measurements of the crystalline micellar ordering's mosaic width as the **10** and **$\bar{1}$ 1** diffraction signals are rotated through the Ewald sphere. The $\omega=-90^\circ$ data (incident beam perpendicular to the flow direction) still clearly shows the **01** and **02** diffraction spots. This geometry is roughly equivalent to the Couette cell geometry case A, of figure 1.

Fig. 9 Flow on minus flow off differential cross-section for in-solution scattering for the 20 mM HC system. The poor subtraction cancellation of the much larger reflected beam signal in this data is due to instrumental shifts over the very long run times (~ 10 hr).



Couette



Poiseuille

Fig 1.

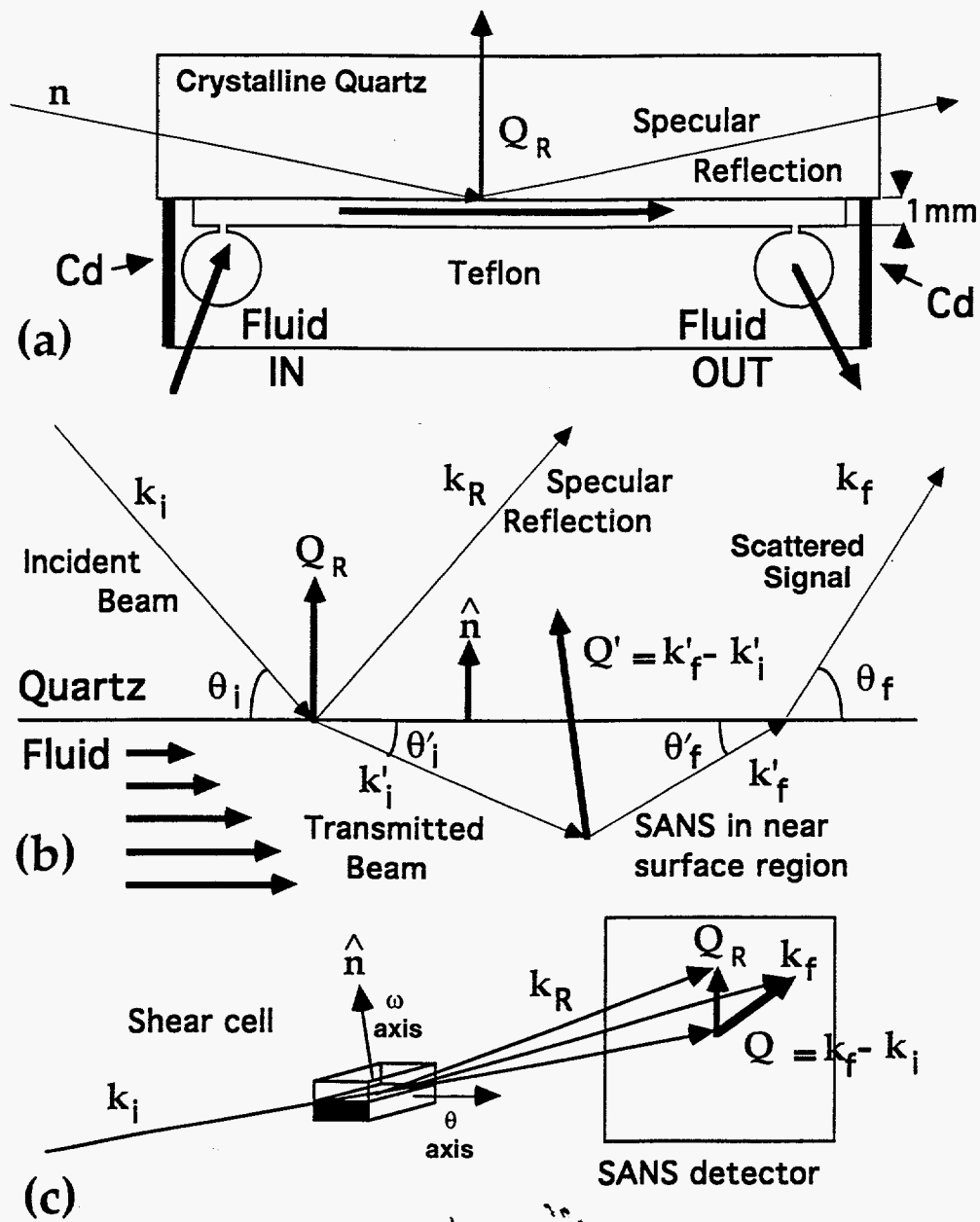
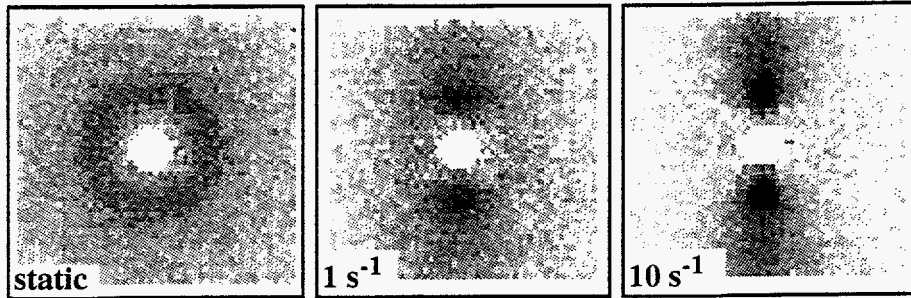


Fig 2.

20 mM MC 70/30



→ Flow direction ($Q_{||}$) →

20 mM HC

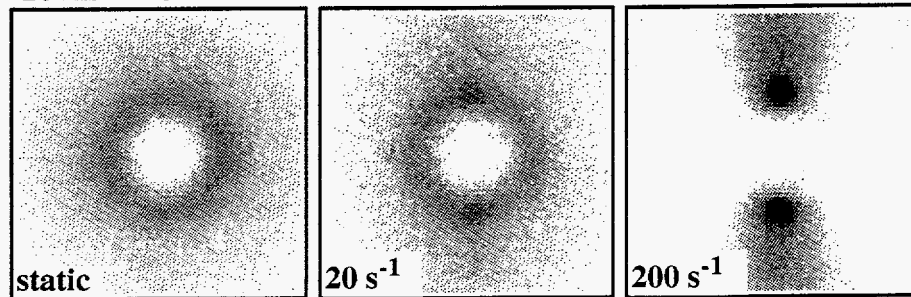


Fig 3.

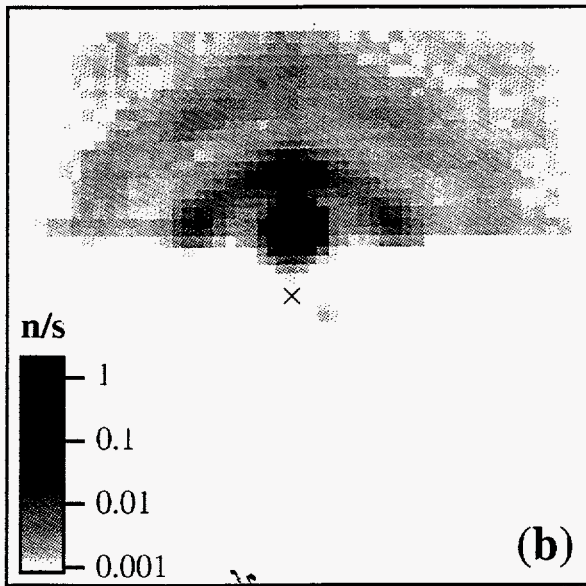
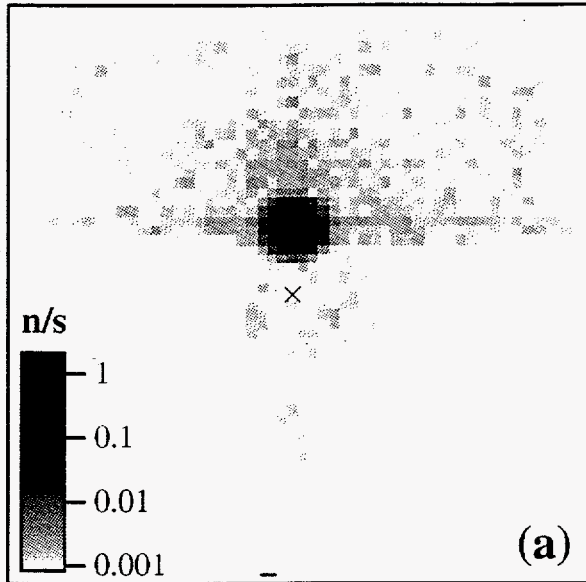


Fig 4.

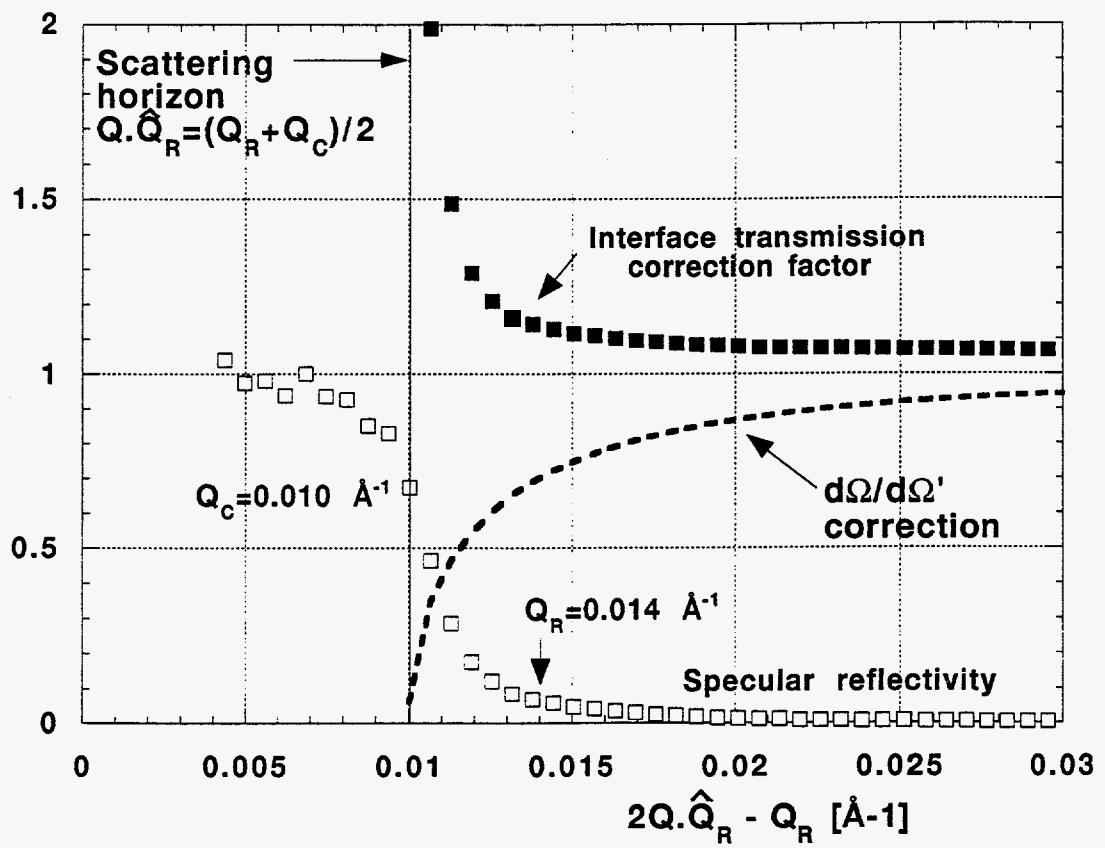


Fig 5.

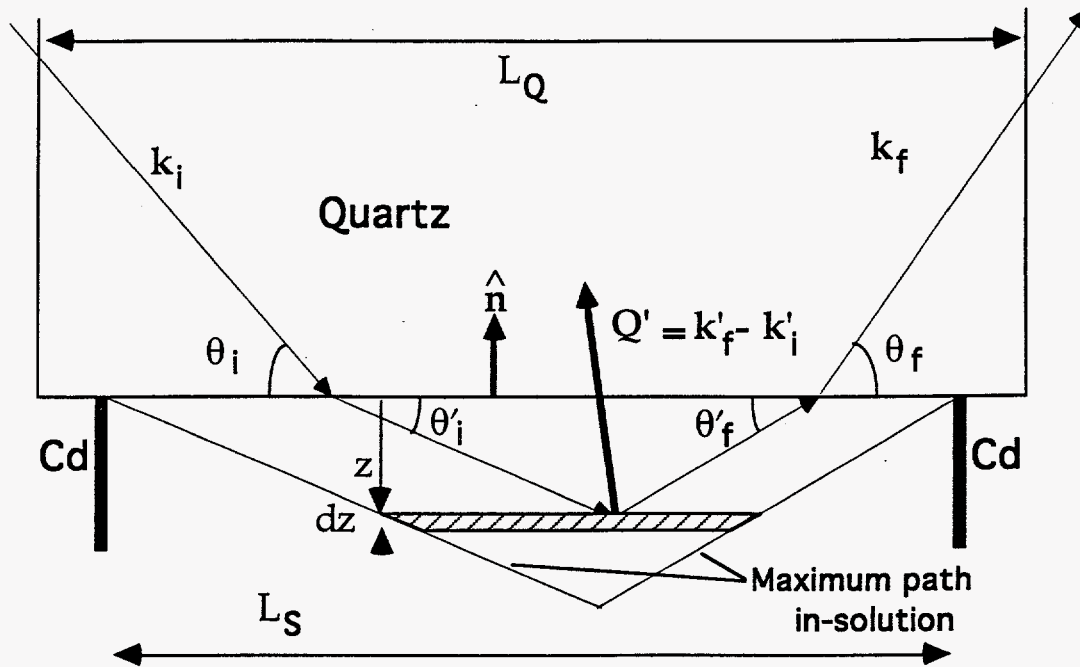


Fig 6.

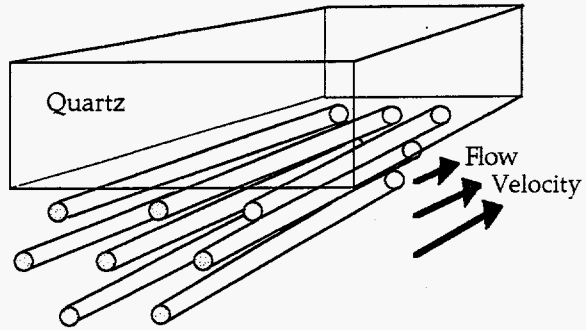
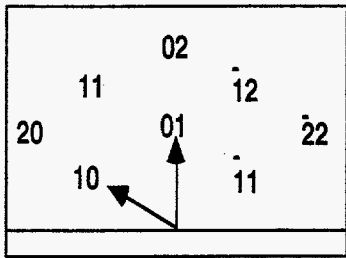
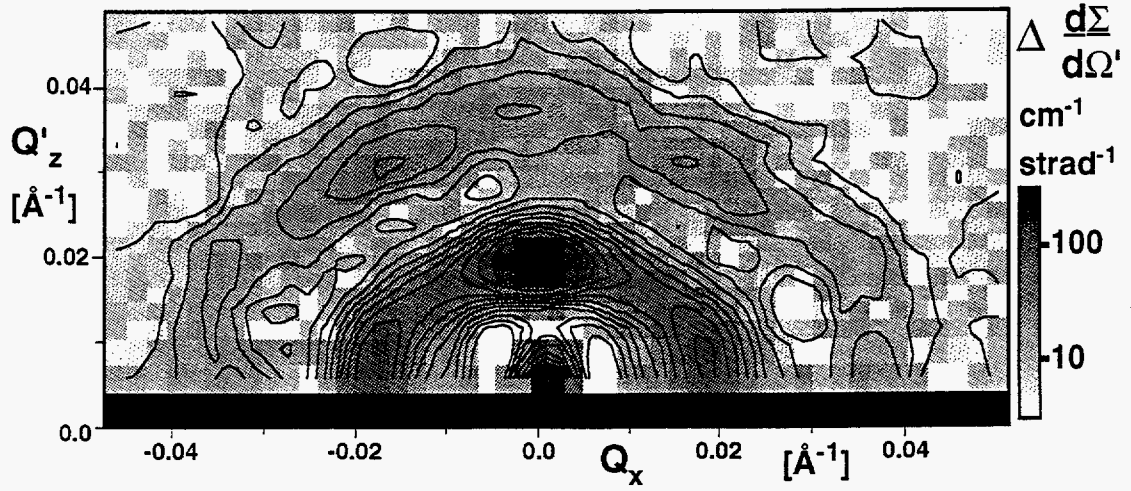


Fig 7.

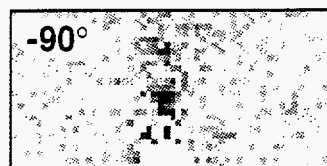
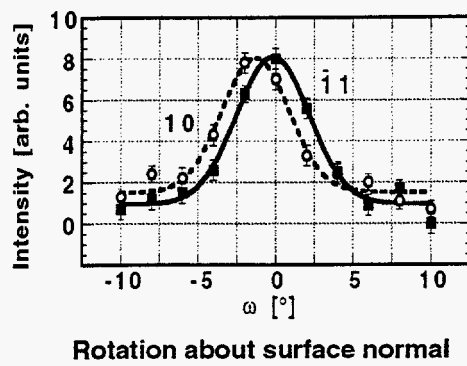
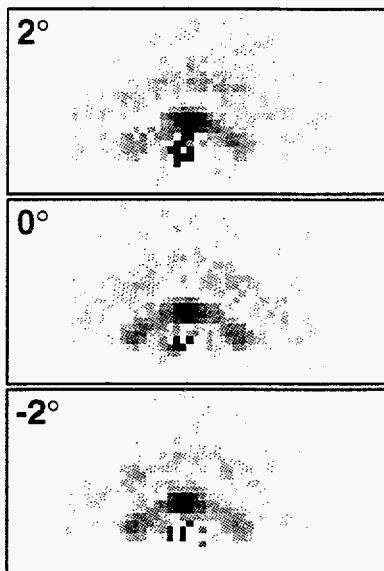


Fig. 8.

Fig 9.

